A Task-Aware Lightweight Link Design Framework for Robots Under Dynamic Loading

Mehmet C. Yildirim[1], Edgar Alejandro Pisano[1], Mazin Hamad[1], Valentin Le Mesle[1], Abdalla Swikir[1,2], and Sami Haddadin[1]

Abstract— **The demand for robotic applications involving dynamic motions in environments with frequent contact is steadily rising. Since these applications also require human-friendly, safe, and robust collaborative operations, the need for more dynamically capable lightweight robots is increasing. Although the current trend is focused on elastic joint-rigid link robot models, the contact task performance can be improved with better modelling and identification of link structures. In this paper, we explore the critical design parameters of links that affect the robot at the system level by creating a relationship between the high-level task requirements and the component-level ones, i.e., the links. Considering the system's life and application needs, we proposed a three-layer design routine for robot links under dynamic loadings. Moreover, we validated the proposed link structure with Finite Element Analysis (FEA) and Experimental Modal Analysis (EMA). The precision of the analytical overall model is validated, and additional acting effects are identified by comparing the EMA with the FEA results. The results show that the flanges and boundary conditions of the link have direct effects on the overall system performance, and these effects can be either controlled or identified to achieve a requirement-matching system for the link design.**

I. Introduction

Contact with the environment is increasingly becoming an intrinsic part of diverse application areas in which robots are currently being deployed [1]. Among the major robotic applications, one can identify many activities that exploit contact, such as walking, running, and impact-aware manipulation, see Fig. 1. In general, contact-rich tasks are subject to kinematic and force constraints like friction, stiffness, and manipulability. On top of these constraints, systems intrinsically need to integrate highly dynamic loading cycles [2], [3]. However, as of today, robots cannot still execute dynamic contact tasks that require high-frequency operational bandwidth [4] and, if not appropriately addressed, these externally triggered high-frequency events can cause destructive outcomes.

In the literature, tasks requiring interaction with the environment are performed mainly using advanced control strategies, ranging from pure impedance control [9]–[11] to hybrid versions for position-impedance-force tasks [12], [13]. These control strategies can also enable active and passive compliance by including compliant joints [14]–[16]. For human-robot collaboration tasks, torque control is applied to lightweight serial robots (e.g., Universal Robot (UR) family, DLR/Kuka Lightweight Robot (LWR) arms, Franka Emika robots) equipped with internal sensors to generate the desired trajectories and interactions [17], [18]. This combination of torque control, lightweight structures, and embedded sensors minimizes the mass and inertial properties of the system, which in turn reduces the applied wrench on the end-effector caused by the motion and the system's inertia [19]. Hence, lightweight, compliant, and actively torque-controlled systems are promising solutions for contact-rich robotic tasks.

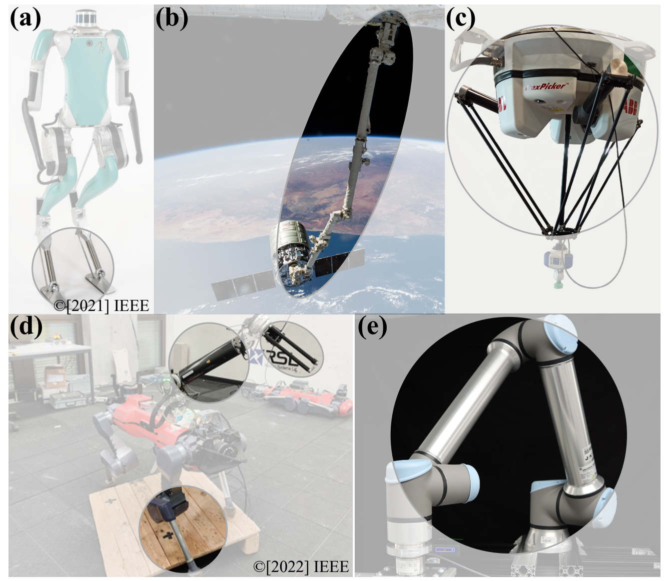

Fig. 1. Examples of robotic systems capable of physical contact with beam-like link structures [5]–[8]. All the highlighted link structures can be designed with the design methodology detailed in this paper.

Contact-rich applications are currently clustered under two separate domains. The first one, later denoted *high-level*, consists of extracting constraints from the task. The second, later denoted *low-level*, consists of defining the design parameters of the components. These two levels can be combined by describing the robot as a 'mid-level' system, which includes the stiffness of the components. Indeed, studies on elastic joints (EJs) evaluate the impact of joint stiffness on the task. This parameter is also used to find a compromise between joint mass and its actuation capabilities. While fewer studies

This work was partially supported by the European Union's Horizon 2020 research and innovation programme as part of the project Darko under grant no. 101017274 and partially supported by the funding of the Lighthouse Initiative KI.FABRIK Bayern, (Phase 1: Infrastructure as well as the research and development program under, grant no. DIK0249), by the Bavarian State Ministry for Economic Affairs, Regional Development, and Energy (StMWi).

[1] All authors are with the Munich Institute of Robotics and Machine Intelligence (MIRMI), Technical University of Munich (TUM), 80797, Munich, Germany. e-mail: {firstname.surname}@tum.de

[2] Abdalla Swikir is also with the Department of Electrical and Electronic Engineering, Omar Al-Mukhtar University (OMU), Albaida, Libya.

have been carried out on the impact of stiffness on the design of robot links, a recent study from Van de Pierre et al. [20] shows that reducing the link stiffness can increase its load capacity. However, it induces vibrations, affecting the robot's performance, especially for dynamic loading scenarios. This brings the need for a top-down design framework of the robot links, which uses its stiffness to improve the robot's performance while guaranteeing that the natural frequency responses of the system do not affect the feasibility of the task.

In this paper, we investigate the boundary-defining points on the link that affect the robot at the system level by creating a relationship between the high-level task requirements and the design of the robot links. Further, the application case with dynamic loading presented in [3] is used to showcase a demo use of the framework we are suggesting. The contributions that we achieved can be listed as

- Proposing a hierarchical structure between joint and link for the link design.
- Developing a methodological relationship between the link mass and the constraints of frequency response (FR), stiffness, and lifespan expectancy.
- Proposing a component-level design routine for robots integrating at least one elastic link (EL) under dynamic loading.
- Highlighting the significance of the boundary conditions (BC) on the EL modelling and identification.
- Validation of link FR models with Finite-Element Analysis (FEA) and Experimental Modal Analysis (EMA).

This paper is structured as follows. First, Sec. II presents the current state-of-the-art on the modelling of robot joints and links, followed by our proposed modelling framework detailed in Sec. III. The precision of the analytical model is validated, and additional acting effects are identified in Sec. IV by comparing EMA and FEA results, while further results are discussed in Sec. V. Finally, Sec. VI concludes the paper and suggests future research directions.

II. State-of-the-art

This paper aims to bring a new perspective on the modelling and design of robot links to improve control performances for contact-rich tasks. Currently, three main methods are used to model a robot for such applications. The first considers flexible joints and rigid links (EJ/RL), and the interactions with the environment are evaluated via the joint stiffness [21]. Although these systems can solve safety- and collaboration-related issues, dynamic loading cases have yet to be resolved. A second method describes robots as rigid-joints/elastic-links (RJ/EL) structures. Although this strategy is successful for low-stiffness continuum systems, its application to the manipulation field is limited to 1 to 3 DoF systems with end-effector contact while the focus is on the control of the EL's vibrations, or for manipulators equipped with complex additional sensors, [22], [23].

The third method considers the elasticity of both joints and links in EJ/EL robotic systems. EJ/EL structures have been suggested to better model relatively rigid-link flex-joint robots and to lower the uncertainties during dynamic motions [24], [25]. However, in these studies, the loading and deflections on the links are limited to one-DOF bending. Therefore, the torsional and shear characteristics of the loadings and deformations are mostly neglected, which can be a source of inaccuracy for many applications.

According to Cannon and Schmitz [26], the effects of link flexibility are significant for thin and lightweight links. Various strategies have been proposed to derive dynamic models of flexible links [27], such as the Lumped Parameter Method (LPM), the Assumed Mode Method, the Finite Element Method (FEM), the Transfer Matrix Method, and the Pseudo-Rigid Bodies method, and are mainly used to design controllers. On the other hand, from a design perspective, flexible link robot models can be used to optimize the design parameters of robots. Several studies on the effects of link design on the overall structural dynamics of the system have been introduced [28]–[30]. For instance, Naveen and Rout model the effects of different uncertainties (such as manufacturing imprecisions, link flexibility, and assembly errors) on the system-level structural dynamics [31]. Srinivas and Javed suggest a topology optimization method to reduce the overall mass of the link [32]. However, this study is limited to static loading cases and may not be adapted for dynamic loading scenarios. Although EJ systems can be constrained with a single DoF, EL's continuous elasticity acts as a multi-DoF system and may lead to more complex dynamic modes and dynamic responses. Various methods have been proposed to detect these responses and control such systems [20]. However, since external effects can change the BCs of the link, further investigation might be done to perform tasks involving physical Human-Robot Interaction.

The dynamic models of flexible links can be derived from beam theories, such as the Bernoulli [33], [34] and the Timoshenko beam theory [35]–[38]. Although the Bernoulli beam theory is sufficient for planar-type structures [38], the Timoshenko beam model further includes the effects of rotary inertia and shear deformation, leading to better accuracy [36]. Nevertheless, modelling works mostly remain at the analytical level or are validated via simulations, and application-oriented work is limited to cantilever-beam-like topologies for EL robots. While EJ/RL models are sufficient for various control tasks, improving the EL models may improve the accuracy and extend the bandwidth of these controllers. As such, we propose a design-oriented method to describe robot links, which considers its topology and is validated via experiments. This framework, detailed hereafter, divides the link into subcomponents modelled using the Timoshenko theory. By considering its broad use cases [39], an application for a tubular link subject to boundary constraints is later presented.

III. Methodology

The design procedure presented in this paper is illustrated in Fig. 2. Similarly to the design routine shown in [40], our presented design procedure consists of solving an

Fig. 2. Flow diagram of the suggested routine. The main focus of this study, highlighted with the orange box, divides the design routine into three main steps. The first, noted (a), uses the task requirements and design constraints to build an initial link design. The second step (b) is a solution process, which aims to ensure that the FR of the link and its lifetime fits with the task requirements. Finally, an experimental validation is performed in step (c).

optimization problem where the design parameters, BCs, and objective function are derived from high-level requirements. It also integrates low-level specifications, such as joint requirements and design decisions related to the link topology (outer radius of the flange R_f and inner radius of the link R_i). The proposed methodology is based on three main properties and constitutive constraints: (i) stiffness, (ii) frequency response, and (iii) link lifetime. While stiffness is the main parameter used in this method, the FR of the link is affected by its structure and the BC applied to the system. As a result, the FR is used as a constraint for the design routine. The lifetime of the link is finally integrated into the method to ensure reliable designs. This section describes the different modules implemented in the design routine. The first subsection details the representation of the link as a subsystem. Then, the evaluation of the link's stiffness, FR, and fatigue effects are presented in three subsections. A subsection is then dedicated to the use of the FEM as a ground truth to validate the analytical models. The implementation of these models inside a solution routine is detailed.

A. Link Definition

Typically, as depicted with red beams in Fig. 3, the links of EJ/RL robots are considered as rigid bodies that connect a joint J_i to an actuator A_{i+1}. On the other hand, EL robots are characterized by the distributed elasticity/stiffness between these two frames. The link is then described as a single part, and its stiffness, denoted as k_{LC} in Fig. 3, controls the system. From our perspective, a more accurate model can be obtained by considering the connection flanges in J_i and A_{i+1} as individual parts, and by defining the link as the body that connects the two flanges. Such description implies the introduction of the flange stiffness and the link body stiffness, expressed as k_f and k_L, respectively. However, since the main control focus is on the joint elasticity k_j and the task-level requirements (e.g., workspace and loading cycles) dictate overall design parameters, we believe that k_{LC} has to be calculated separately, and as dependent on k_j and task-level requirements. Therefore, flange parameters and k_f can be design parameters and act as BCs.

This study focuses on k_L and the link's FR. The BCs are selected based on a mass-spring structure represented in Fig. 3, where we focus on the clamped-free case as suggested by [24], [25]. Additionally, the mass of each flange is modelled as a tip mass, as described in [38]. Furthermore, the inner (R_i) and outer (R_o) radii of the tube are selected as the only independent design parameters. As joint parameters are prioritized over the link dimensions, the joint flange's size dictates the maximal acceptable value of the link's outer radius, noted $R_{o;max}$. Additionally, since the links are also used as a casing for the inter-joint cable harness, the minimum acceptable inner link radius ($R_{i;min}$) is selected as a design constraint. All the defined parameters of the proposed topology are displayed in Fig. 4.

In accordance with [24], on a system with multi-DoF serial structure with rotational joint and beam-like link elasticities, the stiffness of the overall system can be calculated with decoupled individual component elasticities so that the individual stiffness of a component does not affect the other. Therefore, the relative planar displacement between two consecutive actuators A_{i+1} and A_i can be calculated as the sum of the deflection of each sub-component. As a result, the position y_{i+1} of the actuator A_{i+1} with respect to the position y_i of the actuator A_i can be computed as:

$$y_{i+1} = y_i + (L_j + L_f) \sin q_i + L \sin \theta_f + w_L \qquad (1)$$

where L; L_j; and L_f are respectively the length of the link, joint, and flange, while q_i and θ_f are the joint angle and flange deflection angle respectively with deflection of the link body w_L.

B. Stiffness Modelling

The solution routine depicted in Fig. 2 requires an initial value of k_L, which is approximated here via the LPM presented in [41] such that:

$$k_L = \frac{3EI}{L^3} = \frac{3E\pi(R_o^4 - R_i^4)}{4L^3}; \qquad (2)$$

where E corresponds to the Young modulus of the material, and I is the second moment of area. For this parametrization,

Fig. 3. (a) The 3D representation of the considered structure of an n-DoF serial robot where each link, depicted in red. (b) The control model simplifaction where the overall stiffness is considered as k_{LS}. (c) The suggested new link definition where each link is modelled as a mass-spring system. This model integrates the stiffness of the flanges and of the link separately, respectively named k_{fl} and k_L, while considering the overall stiffness for the control model as k_{LC}.

Fig. 4. (A) Tubular link topology used in this paper with its design parameters. (B) Simplified link flange mass values with the used BCs. (C) Kinematic deformation of a cross-section dx adapted from [38].

the flange stiffness is decoupled, and the impact of the transition between the flange and the link body is neglected.

As the stiffness of the link is a design parameter, the Timoshenko method is used to evaluate the natural frequencies based on the stiffness k_L. We employ the Timoshenko method for stiffness modelling as introduced in [42] and briefly reviewed below[1]. The deflection w is given based on the loaded moments on the beam M ($\in \mathbb{R}$) and the shear forces $V \in \mathbb{R}$, whereas $x \in [0, L]$ is the position along the link length (L) and time (t). By noting the rotation of the cross-section as φ and w as the beam deflection, Loudini defines total internal bending and shear forces as [38],

$$M(x,t) = EI\,\frac{\partial \varphi(x,t)}{\partial x}; \tag{3}$$

$$V(x,t) = \kappa GA\left(\frac{\partial w(x,t)}{\partial x} - \varphi(x,t)\right); \tag{4}$$

where κ is the shear correction ratio, $G \in \mathbb{R}$ is the modulus of rigidity and $A \in \mathbb{R}$ is the cross-sectional area of the beam. Furthermore, the changes of M and V w.r.t. to position $x(t)$ are defined by the Timoshenko method as follows:

$$\frac{\partial M(x,t)}{\partial x} = V(x,t) + \rho I\,\frac{\partial^2 \varphi(x,t)}{\partial t^2}; \tag{5}$$

$$\frac{\partial V(x,t)}{\partial x} = \rho A\,\frac{\partial^2 w(x,t)}{\partial t^2}; \tag{6}$$

where $\rho I(\partial^2 \varphi(x,t)/\partial t^2)$ is the distributed rotational inertia, $\rho A(\partial^2 w(x,t)/\partial t^2)$ is the distributed transverse inertial force, while ρ is the material's density. The general solution for the free vibration of the link is [42],

$$\begin{aligned} M(x) = {} & A_1 \cosh(\lambda_1 \tfrac{x}{L}) + B_1 \sinh(\lambda_1 \tfrac{x}{L}) \\ & + C_1 \cos(\lambda_2 \tfrac{x}{L}) + D_1 \sin(\lambda_2 \tfrac{x}{L}); \end{aligned} \tag{7}$$

[1] For the sake of brevity, we give only the final solutions of the proof given in [42].

C. Frequency Response Modelling

where A_1, B_1, C_1, and D_1 are the integration constants evaluated such that the selected BCs match those in w, φ, M, and V. The pair of roots λ_1 and λ_2 is defined as

$$\lambda_1 = \sqrt{\left(-\beta(k_s + k_r) + \sqrt{\beta^2(k_s + k_r)^2 + 4\beta(1 - \beta k_s k_r)}\right)/2};$$

$$\lambda_2 = \sqrt{\left(\beta(k_s + k_r) + \sqrt{\beta^2(k_s + k_r)^2 + 4\beta(1 - \beta k_s k_r)}\right)/2};$$

where β is a coefficient proportional to the angular frequency ω, k_r is the coefficient of rigidity, and k_s is proportional to the shear forces affecting the bending. These coefficients can be calculated as

$$\beta = \frac{\omega^2 \rho A}{EI};\; k_r = \frac{I}{AL^2};\; k_s = \frac{EI}{\kappa GAL^2}; \tag{8}$$

where ω is the angular frequency. To define the BCs of the aforementioned analytical model, FEA solutions are used as the ground truth. After working with different BC options, fixed-free BC with the flange as the tip mass is selected. The resulting BCs are the following:

$$\forall t \text{ at } x = 0: w(0,t) = 0;\ \varphi(0,t) = 0 \tag{9}$$

$$\forall t \text{ at } x = L: M(L,t) = 0;\ \frac{EI}{L^2} w(L,t) = W; \tag{10}$$

$$(1 - \beta k_s k_r)LV - M(x) = 0; \tag{11}$$

$$LV - \beta m_p W = 0; \tag{12}$$

where W is the tip deflection, m_p is the unified mass of the link (m_L) and mass of the flange (m_f). To find the mode frequencies, BCs are arranged in a coefficient matrix $D \in \mathbb{R}^{n \times n}$ form with the corresponding BC vector $C \in \mathbb{R}^n$ such that

$$\det(D)\,C = 0. \tag{13}$$

where

$$C = [A_1\ B_1\ C_1\ D_1\ W\ LV]^T; \tag{14}$$

whereas the coef cient matrix $D \; 2 \; R^{6 \quad 6}$ is

$$D = \begin{bmatrix} {}_1^2 \; k_r & 0 & {}_2^2 \; k_r & 0 & 0 & 0 \\ 0 & a_1 & 0 & a_2 & 0 & 0 \\ \cosh(\;_1) & \sinh(\;_1) & \cos(\;_2) & \sin(\;_2) & 0 & 0 \\ a_3 \cosh(\;_1) & a_3 \sinh(\;_1) & a_4 \cos(\;_2) & a_4 \sin(\;_2) & & 0 \\ a_5 \cos(\;_1) & a_5 \sin(\;_1) & a_6 \cos(\;_2) & a_6 \sin(\;_2) & 0 & a_7 \\ 0 & 0 & 0 & 0 & \frac{(M\;\;)}{(AL\;\;)} & 1 \end{bmatrix}; \quad (15)$$

with $a_i = \;{}_i^2(\;\;{}_i^2 + \;\;(k_r + k_s))\,;\, i \; 2 \; [1;2]$, $a_3 = (\;\;{}_1^2 \;\; k_r)$, $a_4 = (\;{}_2^2 \;\; k_r)$, $a_5 = \;_1(1 + k_r^2 \;\; + k_r \;{}_1^2)$, $a_6 = \;_2(\;1 \;\; k_r^2 \;\; + k_r \;{}_2^2)$, $a_7 = \;\; 1 \;\;\; k_s k_r$.

D. Fatigue Modelling

To check whether the link can hold its consistency for the long term, the lifetime of the link is modelled using Palmgren-Miner's rule [43]. The total damage given by a speci c fully-reversed loading cycle is thus de ned as

$$D = \sum_{i=1} \frac{n_i}{N_i}; \qquad (16)$$

where n_i is the cycle repetition number and N_i is the cycle level of a given fatigue stress value $Sf_i \; 2 \; [S_{ut} \; S_e]$, where S_{ut} and S_e are the ultimate and endurance strength of the material [43]. Considering that each continuous loading happens within 10^3 cycles, we get:

$$N_i = \left(\frac{Sf_i}{a}\right)^{1=b} : \; a = \frac{(f S_{ut})^2}{S_e}; \; b = \;\; \frac{1}{3}\log \left(\frac{f S_{ut}}{S_e}\right); \qquad (17)$$

with f being the fatigue strength fraction. To nd the stress values, a relationship between the loading and the resultant stress should be established. Using $M(x;t)$, the bending stress is calculated as

$$_{b;max}(x;t) = \frac{M(x;t) y}{I} \quad (1 + q(K_t \quad 1)); \qquad (18)$$

where K_t is the stress concentration factor and q is the notch sensitivity. By considering the uctuating loading cycles, the peak counting method is used to determine the stress levels, and the Gerber fatigue criterion [43] is used to de ne the fatigue stress for a given stress level i such that

$$Sf_i = \begin{cases} \dfrac{a}{1 \quad (\frac{m}{S_{ut}})^2}; & m > 0 \\ S_e; & m \quad 0 \end{cases} : \qquad (19)$$

where the $_a$ and the $_m$ are the amplitude of the stress at a given cycle and the average stress, respectively.

E. Finite Element Model

The FEM employed in this study has multiple roles: calculating the ange stiffness k_f, providing a validation ground truth to evaluate the analytical models given in Sec. III-B and Sec. III-C, and providing a comparison medium between the experimental validation and the model. To calculate the effect of the realistic BC, fasteners were modelled as elastic bars and included in the overall model of the ange system. Afterward, to validate the analytical solution, a single body FEM of the link is created with tetrahedral elements in the software Ansys Mechanical FEA, while the perfect xed-free BCs are provided and solved with a unit force response.

Fig. 5. Steps of the frequency checking process. (a) The loading values on the link tip w.r.t the task. (b) Frequency values obtained after performing a Fast Fourier Transformation (FFT). (c) Frequency analysis results of the link. (d) Comparison between the values obtained on (b) and (c). The green area shows the acceptable range for the RF of the system, and the orange area corresponds to the undesired values for the system's RF.

Finally, a merger of the link model and the ange model is used to compare the results with the experimental validation method given in Sec. IV. However, it must be mentioned that to avoid any inaccuracy and, to be closer to reality, sensing elements are also modelled as lump masses.

F. Solution Routine

Finally, the previously constructed modules are arranged in a solution routine. Since the total mass of the link (m) has a signi cant impact on the interaction with humans and on collisions/safety [17], the function f which is used to calculate them was chosen as the cost function to be minimized such that:

$$\begin{aligned} m \;\; &:= \min f(R_i; R_o) \\ \text{s.t. } R_i \; 2 \;\; &; R_o \; 2 \;\; ; \end{aligned} \qquad (20)$$

where and are the box constraints for the decision variables R_i and R_o, respectively. The proposed solution routine is designed to run at three consecutive levels, detailed hereafter. Being the term required for task-level control studies, the stiffness of the link is selected in a case-speci c manner. For example, in an EJ robot, the stiffness of the rigid components has to be signi cantly higher than the stiffness of the joints. Therefore, our link stiffness is selected as the rst constraint, where k_d is the minimum acceptable stiffness value for the link such that

$$k_d \quad k_L: \qquad (21)$$

At the rst stage of the routine, the k_L value is selected such that R_i, de ned by the function g, is minimized as

$$\begin{aligned} R_i \;\; &:= \min g(R_o; k_L) \\ \text{s.t. } R_o \; 2 \;\; &; k_L \; 2 \;\; ; \end{aligned} \qquad (22)$$

and the box boundaries (;) are de ned by choosing the minimum inner radius ($R_{i;\,min}$) as a design factor. Many use cases may affect this value, such as manufacturing, harnessing requirements, etc. On the other hand, integrated joint design is considered another boundary-de ning factor for the ange sizes. Therefore, the maximum outer radius ($R_{o;max}$) is de ned based on R_f with a threshold value. Thus, $\;2\; (R_{i;\,min}; R_{o;max}]$, $\;2\; [R_{i;\,min}; R_{o;max})$, and $\;2\; [k_d; 1\;)$. The calculated values $R_{i;\,min}; R_{o;max}$ are later used to solve the eigenvalue problem of the coef cient matrix (15) to estimate the resonance frequency of the system. Later,

Fig. 6. Flowchart of the validation procedure. The rst evaluation step compares results obtained from the analytical model and FEA. After validation, a link specimen is manufactured, and experimental results are compared with simulation results. The lifetime of the link is taken into account by modifying the BC.

TABLE I
PROPERTIES OF THE LINK SPECIMEN

Input Values				
Design Parameters				
L (mm)	L_f (mm)	E (Pa)	G (Pa)	(kg=m^3)
370	5	$71{:}710^9$	$26{:}910^9$	2810
Boundary and Constraint Parameters				
R_f (mm)	$R_{i;min}$ (mm)	k_d (kN/m)	$!_{i;1}$ (Hz)	$!_{i;2}$ (Hz)
34.5	10	100.0	150.00	250.00
V (N)	F_{ext} (t) (N)	N_d (-)		
54.9	7 sin(300 t) + 15	1e6		
Output Values				
R_i (mm)	R_o (mm)	k_l (kN/m)	$!_{o;1}$ (Hz)	$!_{o;2}$ (Hz)
20	24	101.5	190.56	1302.71

as shown in Fig. 5, loading data obtained from the high-level study is analyzed via Fast Fourier Transform (FFT) to estimate the dominant frequencies of the loading cycle.

At the second stage of the solution routine, a frequency matching between the computed RF values of the link and the FFT results is compiled. The desired system should have no matching between the FFT results and RF values. It is noteworthy here that, as a safety measure, this comparison is made with a safe boundary value since the routine currently does not include the values of k_f.

At the last stage of the routine, the fatigue life of the link, designed with the calculated R_i and R_o, is checked for the desired life cycle of N_d by using (17).

IV. VALIDATION

The proposed methodology is validated with EMA by comparing the accuracy of the link stiffness and its FR to various loadings [44]. Although EMA has different approaches, we selected the impact testing approach to get information for a broader range of frequencies [45]. The validation scenario, illustrated in Fig. 6, is performed as follows. First, a comparison is made between the analytical model solutions and the FEM results. Subsequently, the fatigue is estimated using the analytical model by updating the BCs. Then, experimental results are compared against the FEA results. The test is performed with two different BCs: free-free and xed-free. The free-free BC was approximated by suspending a link specimen with lightweight elastic ropes. For the xed-free case, the specimen is attached to a platform with screws (see Fig. 7).

A case study for the entire routine and the validation procedure is executed with the L and L_f values inspired by the UR5 robot [46], where the obtained solutions and the generated EL system are gathered in Table I. The length of the link and the ange size are selected approximately based on the given DH value for the Link 3 of the UR5 robot. The remaining parts are considered as payload and included in the calculation as continuous static load. In addition, the frequency boundaries are selected based on the sanding operation given in [3]. The resultant geometry is manufactured with an aluminum alloy (EN-AW7075) and performed through physical tests.

As shown in the experimental setup presented in Fig. 7, ve Kistler 8763B series triaxial accelerometers (labelled AC_i) were placed on the link specimen with a gap of 75 mm starting from the clamped base (right side of the free-free BC). The used sensors have a calibrated accuracy of 100 mV/g and a mass of 6 g. A Siemens LMS DAQ system with 24 channels was used to collect the test data. As mentioned in Sec. III-E, the ve sensors were included in the FEM as lumped masses.

To provide the required excitation, an impact hammer with 0:3 kg was used with a steel tip, which allows the creation of vibration frequencies up to 2 kHz. Two different positions on the link are selected for the impacts. The rst point is chosen on the same plane lateral AC_5 but with a rotation of 90 with respect to the central axis of the link. The second point is placed with another 90 rotation relative to P_1, as shown in Fig. 7. These tests were performed for both BCs with ve times excitation for each impact point. After each impact, responses of the system were recorded for 1:5 s and post-processed with the Simcenter Testlab Impact Testing

Fig. 7. Experimental setup used for the EMA. The setup to simulate a pseudo-free-free BC, displayed on the left, maintains the link specimen with elastic ropes. The xed-free BC, on the right gure, xes the link to a base with six screws.

Fig. 8. Bode diagram of the link after excitation at point P1, under the xed-free BCs. The green curve is obtained as the result of 10 measurements, and the mode frequencies of the link are marked as vertical lines.